



PAPER • OPEN ACCESS

A scenario for high-temperature excitonic insulators

To cite this article: Huaiyuan Yang *et al* 2022 *New J. Phys.* **24** 083010

View the [article online](#) for updates and enhancements.

You may also like

- [Effects of the dielectric properties of the ceramic–solvent interface on the binding of proteins to oxide ceramics: a non-local electrostatic approach](#)
Alexander I Rubinstein, Renat F Sabirianov and Fereydoon Namavar
- [Fast method for high-resolution holographic 3D display with white light as illumination](#)
Xin Yang, HongBo Zhang, Qiang Song et al.
- [Integral computer-generated hologram via a modified Gerchberg-Saxton algorithm](#)
Pei-Jung Wu, Chien-Yue Chen, Qing-Long Deng et al.



PAPER

A scenario for high-temperature excitonic insulators

OPEN ACCESS

RECEIVED
27 April 2022REVISED
12 July 2022ACCEPTED FOR PUBLICATION
18 July 2022PUBLISHED
11 August 2022

Original content from
this work may be used
under the terms of the
[Creative Commons
Attribution 4.0 licence](https://creativecommons.org/licenses/by/4.0/).

Any further distribution
of this work must
maintain attribution to
the author(s) and the
title of the work, journal
citation and DOI.

Huaiyuan Yang¹ , Xinqiang Wang^{1,2,3} and Xin-Zheng Li^{1,2,3,4,*} ¹ State Key Laboratory for Artificial Microstructure and Mesoscopic Physics, Frontier Science Center for Nano-optoelectronics and School of Physics, Peking University, Beijing 100871, People's Republic of China² Collaborative Innovation Center of Quantum Matter, Peking University, Beijing 100871, People's Republic of China³ Peking University Yangtze Delta Institute of Optoelectronics, Nantong, Jiangsu 226010, People's Republic of China⁴ Interdisciplinary Institute of Light-Element Quantum Materials, Research Center for Light-Element Advanced Materials, and Collaborative Innovation Center of Quantum Matter, Peking University, Beijing 100871, People's Republic of China

* Author to whom any correspondence should be addressed.

E-mail: xzli@pku.edu.cn**Keywords:** excitonic insulator, transition-metal dichalcogenides, electronic structureSupplementary material for this article is available [online](#)**Abstract**

While excitonic insulators (EIs) have been intensively studied, proper platforms of them with stable lattice and non-cryogenic T_C are rare. By analysing their Bardeen–Cooper–Schieffer-like gap equation, we propose that high T_C EIs can exist in small indirect band gap 2D materials. After screening 2D transition-metal dichalcogenides from existing computational works, we select $2H\text{-TiTe}_2$ and $1T\text{-PdTe}_2$, and show that their T_C can be as high as 150 to 200 K under strains. A transition of their condensate EI state from that composed by Wannier excitons to that composed by plasmonic ones exists, even if negligible changes are reflected by the EI band structures, demonstrating the rich quantum feature of these systems. The high T_C also implies that they are ideal platforms for the demonstration and applications of EIs and their related quantum states in non-cryogenic environments.

1. Introduction

The concept of excitonic insulators (EIs) was proposed by Keldysh and Kohn successively in the 1960s [1–3]. It is a correlated electronic state where bound excitons, a kind of bosonic quasiparticle composed by electron–hole pairs, form and condensate spontaneously without the requirement of optical excitations. An EI state can exist if the exciton binding energy E_b exceeds the band gap E_g . In the semimetal region ($E_g \leq 0$), this condition can relax as long as bound excitons exist. In analogy to the superconductivity, EIs can be well described by the Bardeen–Cooper–Schieffer (BCS) theory, except that the excitons take the place of the Cooper pairs. Below the critical temperature (T_C), the EI state forms, which opens a detectable quasiparticle gap. The EIs are perfect insulators for heat and charge transport.

Over the last half a century, EIs have been sought persistently, and there are much progress made in experiment. Two well-known examples are $1T\text{-TiSe}_2$ [4, 5] and Ta_2NiSe_5 [6–8]. However, lattice instability exists in these two materials at low temperatures, making it hard to confirm the excitonic mechanism behind them. Other systems, including InAs/GaSb quantum well [9] and $\text{MoSe}_2/\text{WSe}_2$ bilayers [10], require elaborate processing of the atomic structures, which hinders their further applications. Therefore, more insights for exploring dynamically stable intrinsic EIs are highly desired. In the first place, the realization of EIs calls for large E_b . This requires reduced screening of the Coulomb interactions, which is drastic in low dimensional systems. However, as shown in reference [11], E_g is approximately four times as large as E_b in two-dimension for direct excitons. One way to break this synergy between E_g and E_b is to take advantage of the dipole forbidden transitions near the band edges [12–14]. The second way is to increase the overlap of the electron–hole wave functions, so that they are immune to the screening effect from surrounding charges

[15]. These two strategies have been chosen in several previous works, predicting that 2D GaAs [12], 1T-NiCl₂ [13], graphone [14] and a diatomic kagome lattice [15] are intrinsic EIs with large E_g s but even larger E_b s. Besides them, a third strategy exists in systems with small indirect band gap, as this quadruple relationship does not hold anymore in the indirect case, and therefore E_b of indirect excitons may remain finite even if the indirect band gap is vanishingly small. We followed such a strategy in this study and proved it to be possible from first-principles GW-Bethe–Salpeter equation (BSE) calculations. Moreover, we found it even superior, in the sense that not only EIs can be identified, but also non-cryogenic T_C s can be realised based on a simple logic behind its gap equation. We emphasize that this strategy is feasible practically, as monolayer WTe₂ was shown to be an EI at around 100 K in recent experiments, where the indirect excitons trigger the condensation [16, 17].

To describe the EI transition, the order parameter is defined as:

$$\Delta(\mathbf{k}) \equiv -\sum_{\mathbf{k}'} V(\mathbf{k} - \mathbf{k}') \langle a_{\mathbf{k}'}^\dagger b_{\mathbf{k}'} \rangle, \quad (1)$$

where $a_{\mathbf{k}}(b_{\mathbf{k}})$ is the electron(hole) operator, and $V(\mathbf{q})$ is the screened Coulomb interaction between electrons and holes. The corresponding self-consistent equation in analogy to the BCS gap equation reads [3]:

$$\Delta(\mathbf{k}) = \sum_{\mathbf{k}'} V(\mathbf{k} - \mathbf{k}') \frac{\Delta(\mathbf{k}')}{2E_{\mathbf{k}'}} [f(E_v(\mathbf{k}')) - f(E_c(\mathbf{k}'))]. \quad (2)$$

Here $E_{\mathbf{k}'} = [(\varepsilon_c(\mathbf{k}') - \varepsilon_v(\mathbf{k}'))^2/4 + |\Delta(\mathbf{k}')|^2]^{1/2}$, and $f(x) = 1/(1 + e^{(x/k_B T)})$ is the Fermi–Dirac distribution function. It is clear from (2) that stronger Coulomb interaction $V(\mathbf{q})$ and smaller gap can lead to larger order parameter. In so doing, T_C can be elevated. This motivates us to search platforms for EIs with high T_C in 2D materials with small indirect band gap, where these two conditions are both satisfied.

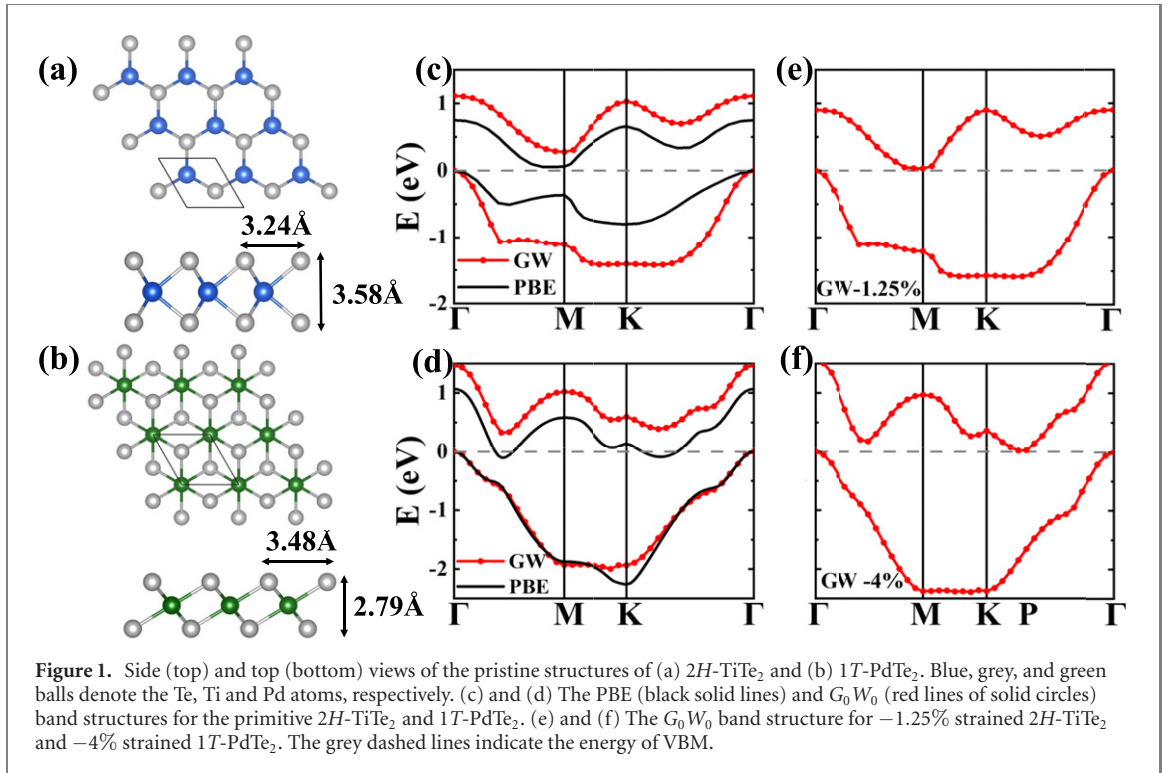
Among the different atomically thin 2D materials, we focus on transition-metal dichalcogenides (TMDs), due to their unique optoelectronic properties [18, 19]. Based on recent computational works [20, 21], many 2D TMDs are screened. We found that 2H-TiTe₂ and 1T-PdTe₂ under strains are high T_C EIs, meaning that they are ideal platforms for the demonstration and applications of EIs and their related quantum states at non-cryogenic temperatures. These conclusions are drawn from first-principles many-body perturbation theory and self-consistent two-band model calculations on top of them. A detailed phase diagram of these systems under varying strains and temperatures is given. By tuning the strain, we see a transition of their condensate EI state from that composed by Wannier excitons to that composed by plasmonic ones, with negligible changes reflected by their EI band structures. This also demonstrates the rich quantum nature of these two materials.

The rest of this paper is organized as follows. We present the computational details of the first-principles calculations in section 2. In section 3, we show the results, including the density-functional theory (DFT) and G_0W_0 band structures, exciton dispersions from the BSE calculations and the phonon spectra. Excitonic instability is found under strains. Then we present the phase diagrams of these two materials using the two-band model together with the renormalized band structures, and high T_C s are shown explicitly. A summary of the main results and some discussions are given in section 4.

2. Computational details

The electronic ground states were computed within DFT using the QUANTUM ESPRESSO package [22]. Perdew–Burke–Ernzerhof (PBE) exchange correlation functional [23] was used in describing the Kohn–Sham exchange–correlation potential, along with a $18 \times 18 \times 1$ k -point mesh for the Brillouin-zone sampling. The kinetic energy cutoff for the wavefunction was set to be 90 Ry, and the fully relativistic version of the SG15 Optimized Norm-Conserving Vanderbilt pseudopotentials [24, 25] were used to take spin–orbit interactions into account. An 20 Å thick vacuum layer was used to avoid interactions between adjacent layers. The lattice was relaxed until the forces on each atom were less than 0.5 meV Å⁻¹, and the relaxed structures for both materials are shown in figures 1(a) and (b). The phonon dispersions were calculated by the finite displacement method using the PHONOPY package [26].

Then we performed many-body perturbation theory calculations using the YAMBO code [27]. We used the G_0W_0 approximation for the self-energy to correct the quasiparticle energies on top of the PBE values. Full-frequency integration method was used to account for the dynamical dielectric screening effects. To converge the band gap within 3 meV, eighty empty bands were included to build the polarizability, and the Brillouin zone was sampled by a $24 \times 24 \times 1$ k -point grid (see the details for the convergence tests in the supplementary materials <https://stacks.iop.org/NJP/24/083010/mmedia>). The kinetic energy cutoffs for the exchange and correlation parts of the self-energy were 50 Ry and 6 Ry respectively. The BSE was solved at



finite momentum Q , where the exciton wavefunction reads:

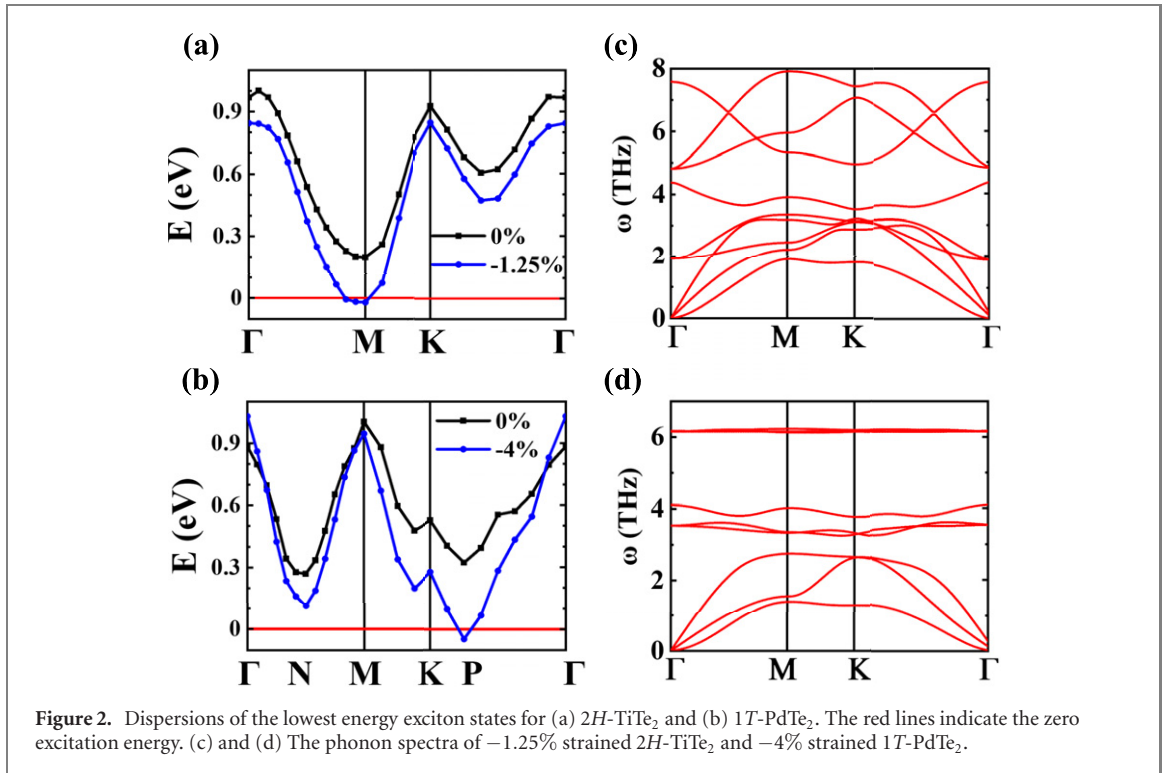
$$\chi^Q(\mathbf{r}_e, \mathbf{r}_h) = \sum_{vck} A_{vk,ck+Q} \psi_{ck+Q}^*(\mathbf{r}_e) \psi_{vk}(\mathbf{r}_h). \quad (3)$$

$A_{vk,ck+Q}$ is the envelope function, and $\psi_{ck}(\psi_{vk})$ is the electron (hole) Bloch wavefunction. The static dielectric function matrix was calculated within the random-phase approximation, with local-field effects included. Forty empty bands and 5 Ry cutoff were used. The same k -point grid as in the G_0W_0 calculations was chosen to achieve the convergence within 1 meV. We only focus on the ground state exciton (the lowest branch) throughout the paper.

3. Results and discussions

The black lines in figures 1(c) and (d) illustrate the DFT band structures at the PBE level for $2H\text{-TiTe}_2$ and $1T\text{-PdTe}_2$. The former is an indirect band gap semiconductor and the latter is a semimetal, with band gap or overlap of 53 meV and 107 meV. Given that PBE tends to underestimate E_g , these band structures were calibrated by the many-body perturbation theory within the G_0W_0 approximation. The results are shown by red lines in figures 1(c) and (d). Both $2H\text{-TiTe}_2$ and $1T\text{-PdTe}_2$ are indirect semiconductors, with band gap values of 276 meV and 387 meV. The valence band maximum (VBM) and conduction band minimum (CBM) locate at Γ and M point in $2H\text{-TiTe}_2$, and at Γ and N point (midpoint of ΓM) in $1T\text{-PdTe}_2$. Then we perform finite momentum BSE calculations to determine the lowest energy exciton states. The dispersions of the lowest exciton branches are shown by black lines in figures 2(a) and (b). EIs require the exciton excitation energy lower than zero, but now it is positive for both materials. Therefore, no excitonic instability occurs.

Strain can induce a significant band gap reduction in 2D materials [28]. Considering the fact that the screened Coulomb interaction and the exciton binding energy E_b depend strongly on the direct band gap instead of the indirect one [12, 29], we believe that scenarios for EIs exist upon applying strains, i.e. moderate strains reduce the indirect E_g to vanishingly small values whilst keep the direct E_g finite, in so doing the values of E_b exceed those of the indirect E_g . Based on this consideration, we perform the GW -BSE calculations for $2H\text{-TiTe}_2$ and $1T\text{-PdTe}_2$ under different strains. We applied the biaxial strain by changing the lattice constants without further relaxing the structure, as in references [12, 20]. The band gap decrease fast with the increase of the strain in $2H\text{-TiTe}_2$. The value of indirect E_g is 219 meV at -0.5% strain, 131 meV at -1% strain, and 28 meV at -1.25% strain. The corresponding E_b for the lowest exciton, on the other hand, remains finite, i.e. 69 meV, 50 meV, and 49 meV respectively under these strains. This indicates



an excitonic instability at -1.25% strain, as shown in figure 2(a), where a negative exciton excitation energy can be seen close to M . For $1T\text{-PdTe}_2$, the CBM moves to the P point ($KP = \Gamma K/4$) at the strains larger than -2% , together with the location of the lowest energy exciton state. E_b and the indirect E_g are 63 meV and 284 meV at -2% strain, 62 meV and 96 meV at -3% strain, and 62 meV and 16 meV at -4% strain. Therefore, exciton instability in $1T\text{-PdTe}_2$ exists at $\sim -4\%$ strain.

In many other candidates for EIs, e.g. $1T\text{-TiSe}_2$ [4, 5] and Ta_2NiSe_5 [6–8], the EI transition is accompanied by the phonon softening, making it difficult to distinguish the mechanism behind experimental signals of the mechanical instability. In figures 2(c) and (d), we show the phonon spectra for $2H\text{-TiTe}_2$ and $1T\text{-PdTe}_2$. Absence of the soft mode means that they are dynamically stable. Therefore, instability, if measured by experiment, should be purely excitonic. In experiments, the gap opening like figures 3(a) and (b) can be revealed by angle-resolved photoemission spectroscopy. Besides, an antiferroelectric texture corresponding to the finite momentum of the exciton can be observed by scanning tunneling microscope etc, like in reference [29].

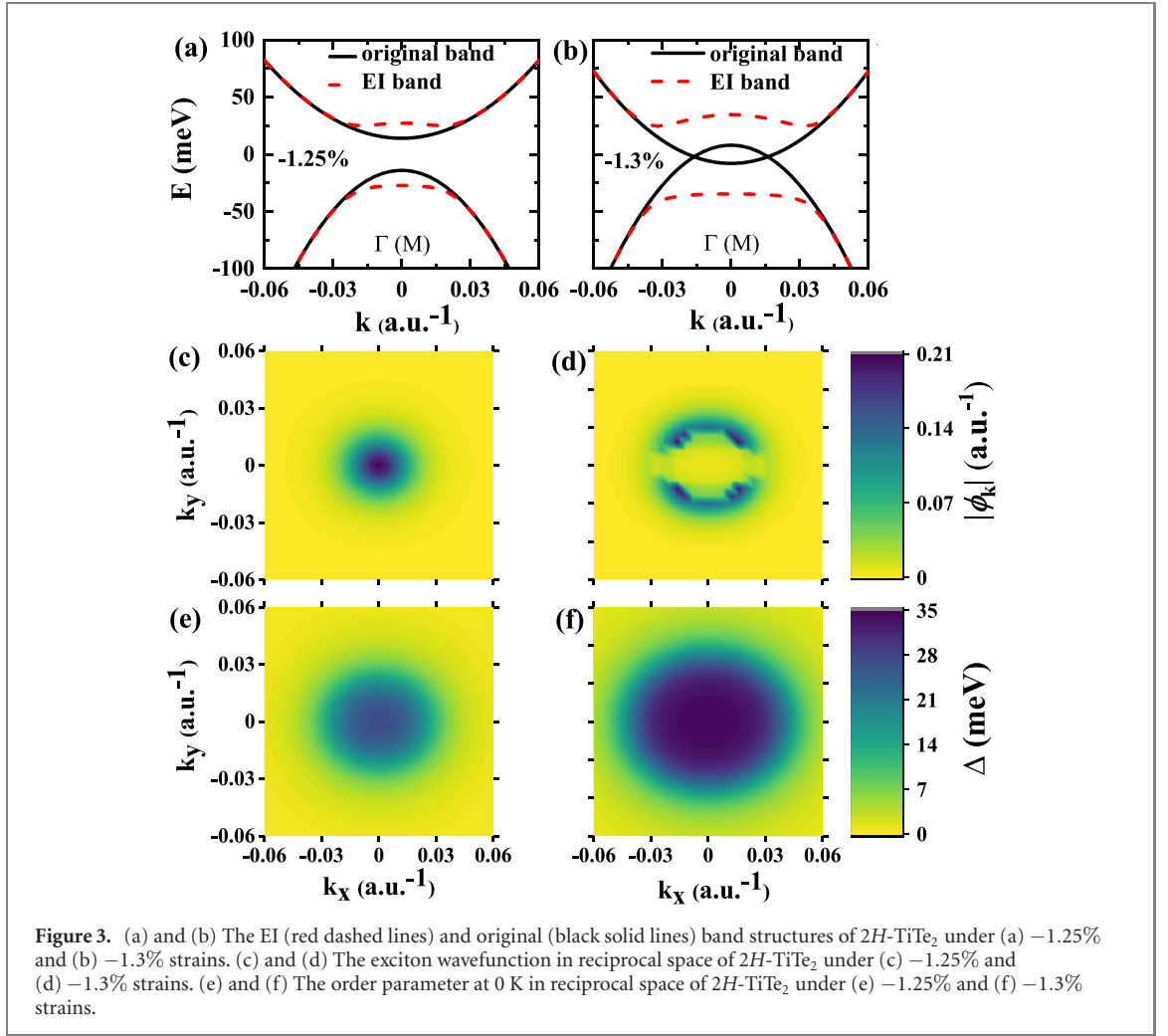
On top of these *ab initio* results, we built a two-band model [29]. As the accuracy of our first-principles calculations for band structure (~ 5 meV) is much larger than the accuracy of the spin degeneracy (~ 0.5 meV) and detailed valley structure (~ 1 meV, see figure 4(A) of reference [29]), we omit the detailed structures of spin and valley degrees of freedom and mainly focus on the transition temperature and the general EI band structures. Despite its simplicity, this model is solid in theory, and the numerical error is very small, as the k -point mesh can be extremely dense. Using this model, the BCS gap equation (2) can be solved so that the order parameter and the transition temperature of the EI state can be obtained. Since $\Delta(\mathbf{k})$ enters both sides of this equation, it must be solved by iterations. EI transition occurs when $\Delta(\mathbf{k})$ has a non-trivial solution.

Besides this, the excitonic states can also be described by this model using the BSE, as detailed below. The Hamiltonian of this two-band model reads:

$$H = \sum_{\mathbf{k}} \varepsilon_c(\mathbf{k}) a_{\mathbf{k}}^\dagger a_{\mathbf{k}} + \sum_{\mathbf{k}} \varepsilon_v(\mathbf{k}) b_{\mathbf{k}}^\dagger b_{\mathbf{k}} + \sum_{\mathbf{k}, \mathbf{k}', \mathbf{q}} V(\mathbf{q}) b_{\mathbf{k}+\mathbf{q}}^\dagger b_{\mathbf{k}} a_{\mathbf{k}'-\mathbf{q}}^\dagger a_{\mathbf{k}'}. \quad (4)$$

From now on, we omit the finite momentum difference between VBM and CBM for convenience. The conduction band and valence band read:

$$\varepsilon_c(\mathbf{k}) = \frac{E_g}{2} + \frac{\hbar^2}{2} \left[\frac{(k_x)^2}{m_x^e} + \frac{k_y^2}{m_y^e} \right], \quad (5)$$



$$\varepsilon_v(\mathbf{k}) = -\frac{E_g}{2} - \frac{\hbar^2}{2} \left[\frac{(k_x)^2}{m_x^h} + \frac{k_y^2}{m_y^h} \right]. \quad (6)$$

The k_x and k_y means the k vector along the Γ - M and Γ - K direction, measured from the CBM and VBM. The m_x^e , m_y^e , m_x^h and m_y^h are the effective masses of the electron and hole along these directions, extracted from the G_0W_0 results together with the indirect band gap E_g and the band overlap. $V(\mathbf{q})$ is the screened Coulomb interaction between the electrons and holes, described by the Keldysh potential in the semiconducting region [30]:

$$V(\mathbf{q}) = \frac{2\pi}{Sq(1 + 2\pi q\alpha_{2D})}. \quad (7)$$

Here $S = 4\pi^2/\Delta q^2$, and Δq is the distance between neighboring k -points on the dense k -mesh. α_{2D} is the 2D polarizability at the momentum of the indirect band gap. When $E_g < 0$ (in the semimetal region), the Coulomb potential will be further screened by the free electron and hole carriers, and $V(\mathbf{q})$ is modified to [31]:

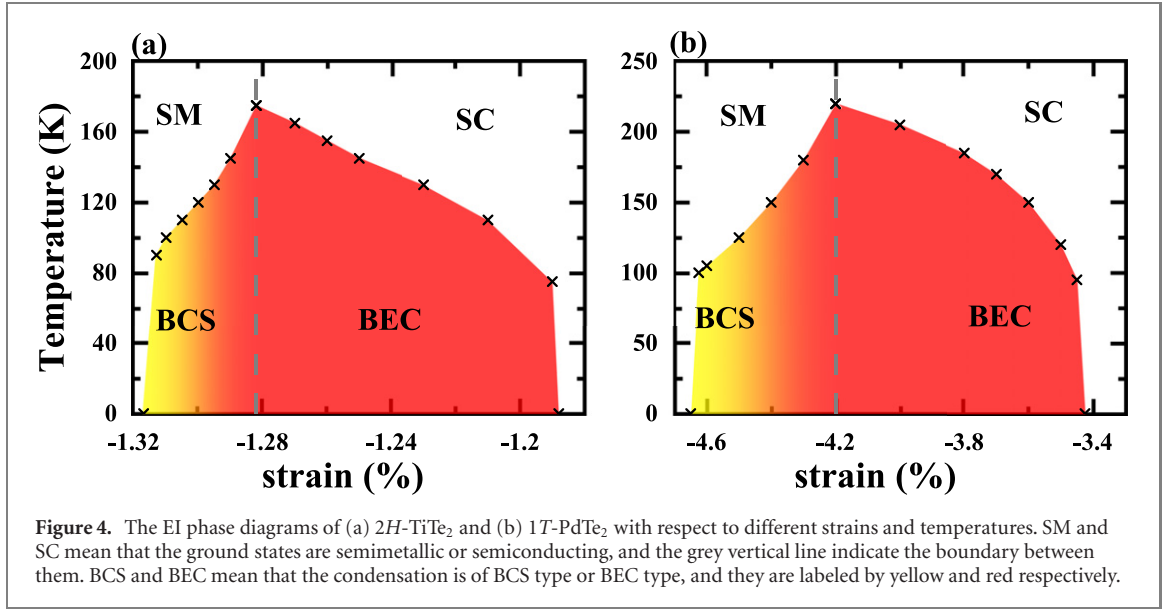
$$V(\mathbf{q}) = \frac{2\pi}{S(1 + 2\pi q\alpha_{2D})} \times \frac{1}{\sqrt{q^2 + \kappa^2}}. \quad (8)$$

κ is the Thomas-Fermi screening factor, fitted by the *ab initio* results. The exciton wavefunction in this two-band model is:

$$\chi = \sum_{\mathbf{k}} \phi_{\mathbf{k}} a_{\mathbf{k}}^\dagger b_{\mathbf{k}} |\Phi_0\rangle. \quad (9)$$

In the semiconducting region, the BSE is written as:

$$(\varepsilon_c(\mathbf{k}) - \varepsilon_v(\mathbf{k}))\phi_{\mathbf{k}} - \sum_{\mathbf{k}'} V(\mathbf{k} - \mathbf{k}')\phi_{\mathbf{k}'} = \varepsilon_{\text{exc}}\phi_{\mathbf{k}}. \quad (10)$$



In the semimetal region, (10) is modified due to Pauli exclusion, reading as:

$$(\varepsilon_c(\mathbf{k}) - \varepsilon_v(\mathbf{k}))\phi_{\mathbf{k}} - \sum_{\mathbf{k}'} V(\mathbf{k} - \mathbf{k}') (n_v(\mathbf{k}') - n_c(\mathbf{k}'))\phi_{\mathbf{k}'} = \varepsilon_{\text{exc}}\phi_{\mathbf{k}}, \quad (11)$$

with $n_c(\mathbf{k})$ ($n_v(\mathbf{k})$) being the occupation number of the conduction (valence) band. The singularity of $V(\mathbf{0})$ can be integrated out. We solve these equations in a very dense k -point mesh to converge the result within 0.1 meV.

In figure 3, we take $2H\text{-TiTe}_2$ as an example to show the EI band structure ($\tilde{E}_k = \frac{\varepsilon_c + \varepsilon_v}{2} \pm E_k$, where E_k is solved in equation (2)), the exciton wavefunctions ($\phi_{\mathbf{k}}$ in (9)), and the order parameters ($\Delta(\mathbf{k})$ in (2)) from the two-band model. When the EI transition takes place, the bands around Γ are replicated at M , and the two bands repel each other, changing the bands from the original parabolas to a quartic-like conduction band and a rather flat valence band. An example in the BEC region is shown in figure 3(a), when the strain is -1.25% . The CBM is slightly shifted from Γ , and the true gap is indirect. Figure 3(c) is the wavefunction of the excitons in reciprocal space, which compose the EI state. The absolute value of the coefficient $\phi_{\mathbf{k}}$ decreases fast to zero when \mathbf{k} is away from Γ , showing a Wannier character with 1s feature. The order parameter at 0 K is also isotropic but more spreading in reciprocal space, as in figure 3(e). After the band gap decreases to zero or minus, the BEC-BCS crossover occurs. We show an example of $2H\text{-TiTe}_2$ at -1.3% strain, where the quasiparticle band structure is semimetal and the band overlap is 16 meV. The EI band structure is similar to that at -1.25% strain, except that the two bands is distorted more (figure 3(b)). The exciton wavefunction, however, is different by showing a plasmonic character which is compressed near the Fermi surface (figure 3(d)). This fact implies that the EI now is mainly of the BCS type. Due to the large effective mass difference in the two directions, there is prominent anisotropy, in sharp contrast to the 1s feature of the exciton in figure 3(c). The absolute value and the shape of the order parameter, on the other hand, still resemble that in the BEC region, which are only a few millielectronvolt larger and more extended in the k -space (figure 3(f)).

To obtain an overall understanding of the phase diagram of these two materials under different thermal and mechanical environment, we run the two-band model simulations for these two materials in a wide range of strains using parameters including the effective masses, the band gaps (overlaps), and the screened Coulomb interactions interpolated from *ab initio* calculations. The results are shown in figure 4. For $2H\text{-TiTe}_2$ ($1T\text{-PdTe}_2$), the EI occurs between -1.317% and -1.188% strain (-4.65% strain and -3.425% strain), and the highest T_C is 175 K (220 K) at -1.282% (-4.2%) strain, when the band gap is zero. In a large strain region, the band gap (band overlap) is relatively small. Therefore, according to (2), the T_C s are very high. The EI states from a semiconducting ground state are highlighted in red and labelled by BEC, meaning that the condensation can be described by BEC of preformed excitons. The EI states from a semimetal ground state, on the other hand, are marked by yellow and labelled by BCS, meaning that the EI transition is in analogy to the BCS superconductors. With more strain, the band overlap grows and the screening effect increases fast, which diminishes the EI state. These intrinsic physical effects do not only promote the emergency of the BCS-BEC crossover, but also induce smaller EI phase space in the semimetal region compared with that in the semiconducting region. Combining these discussion, we emphasize that in

a large EI phase space, the T_C s are high, indicating that these two materials are ideal experimental platforms for the demonstration of the EI state at non-cryogenic temperatures.

However, there are several technical difficulties for the synthesis of these two materials in experiments. $2H\text{-TiTe}_2$ has only been synthesized successfully on Au surface and $1T\text{-PdTe}_2$ needs a large strain to achieve EI. We hope these issues can be overcome in actual experiments, or, in other way, the method we proposed may inspire the discovery of more suitable materials for EI. Recently, references [16, 17] proved that WTe_2 went through an EI transition linked to indirect exciton at around 100 K, in alignment with our expectation.

4. Conclusion

We presented a strategy to seek for high-temperature EIs. Two key factors, i.e., strong Coulomb interaction and small band gap, are extracted from the BCS gap equation. Small indirect band gap 2D materials fulfill these criteria, and we found $2H\text{-TiTe}_2$ and $1T\text{-PdTe}_2$ as two representatives. First-principle GW-BSE calculations showed that they are EIs under strains. The strain-temperature phase diagrams for EI transition obtained from two-band model illustrate that the T_C s are extremely high in a wide range of strain. The BCS-BEC crossover is explicitly observed with respect to the varying strains. The large EI phase spaces for both materials makes them great realistic platforms to study novel phenomenon and explore potential optoelectronic applications of EIs. In particular, as predicted in recent studies [32–34], there will be exotic optical response corresponding to the excitonic collective modes in both linear and nonlinear regime. The correlation effects in EIs may lead to strongly enhanced photovoltaic effects compared to conventional insulators, contributed by a resonating shift current and a nonvanishing injection current [35]. Though charge pumping, arising from order parameter steering in BCS regime, is another novel phenomenon can be pursued in real EIs [36]. We hope more high- T_C EIs can be discovered through this route, inspiring more research including for example the possibility of excitonic high- T_C superconductivity [37].

Acknowledgments

We acknowledge helpful discussions with J R Shi. We are supported by the National Basic Research Programs of China under Grant No. 2021YFA1400503, the Beijing Natural Science Foundation under Grant No. Z200004, the National Science Foundation of China under Grant No. 11934003, and the Strategic Priority Research Program of the Chinese Academy of Sciences Grant No. XDB33010400. The computational resources were provided by the supercomputer center in Peking University, China.

Data availability statement

The data that support the findings of this study are available upon reasonable request from the authors.

ORCID iDs

Huaiyuan Yang  <https://orcid.org/0000-0001-8004-0368>

Xinqiang Wang  <https://orcid.org/0000-0001-5514-8588>

Xin-Zheng Li  <https://orcid.org/0000-0003-0316-4257>

References

- [1] Keldysh L and Kopaev Y V 1965 *Sov. Phys. Solid State* **6** 2219
- [2] Kohn W 1967 *Phys. Rev. Lett.* **19** 439
- [3] Jérôme D, Rice T M and Kohn W 1967 *Phys. Rev.* **158** 462
- [4] Cercellier H et al 2007 *Phys. Rev. Lett.* **99** 146403
- [5] Kogar A et al 2017 *Science* **358** 1314–7
- [6] Wakisaka Y et al 2009 *Phys. Rev. Lett.* **103** 026402
- [7] Lu Y, Kono H, Larkin T, Rost A, Takayama T, Boris A, Keimer B and Takagi H 2017 *Nat. Commun.* **8** 14408
- [8] Mor S et al 2017 *Phys. Rev. Lett.* **119** 086401
- [9] Du L, Li X, Lou W, Sullivan G, Chang K, Kono J and Du R R 2017 *Nat. Commun.* **8** 1971
- [10] Wang Z, Rhodes D A, Watanabe K, Taniguchi T, Hone J C, Shan J and Mak K F 2019 *Nature* **574** 76–80
- [11] Jiang Z, Liu Z, Li Y and Duan W 2017 *Phys. Rev. Lett.* **118** 266401
- [12] Jiang Z, Li Y, Zhang S and Duan W 2018 *Phys. Rev. B* **98** 081408
- [13] Jiang Z, Li Y, Duan W and Zhang S 2019 *Phys. Rev. Lett.* **122** 236402

- [14] Jiang Z, Lou W, Liu Y, Li Y, Song H, Chang K, Duan W and Zhang S 2020 *Phys. Rev. Lett.* **124** 166401
- [15] Sethi G, Zhou Y, Zhu L, Yang L and Liu F 2021 *Phys. Rev. Lett.* **126** 196403
- [16] Sun B et al 2022 *Nat. Phys.* **18** 94–9
- [17] Jia Y et al 2022 *Nat. Phys.* **18** 87–93
- [18] Wang Q H, Kalantar-Zadeh K, Kis A, Coleman J N and Strano M S 2012 *Nat. Nanotechnol.* **7** 699–712
- [19] Nicolosi V, Chhowalla M, Kanatzidis M G, Strano M S and Coleman J N 2013 *Science* **340** 1226419
- [20] Rasmussen F A and Thygesen K S 2015 *J. Phys. Chem. C* **119** 13169–83
- [21] Thygesen K S 2017 *2D Mater.* **4** 022004
- [22] Giannozzi P et al 2009 *J. Phys.: Condens. Matter* **21** 395502
- [23] Perdew J P, Burke K and Ernzerhof M 1996 *Phys. Rev. Lett.* **77** 3865
- [24] Hamann D R 2013 *Phys. Rev. B* **88** 085117
- [25] Scherpelz P, Govoni M, Hamada I and Galli G 2016 *J. Chem. Theory Comput.* **12** 3523–44
- [26] Togo A and Tanaka I 2015 *Scr. Mater.* **108** 1–5
- [27] Sangalli D et al 2019 *J. Phys.: Condens. Matter* **31** 325902
- [28] Fiori G, Bonaccorso F, Iannaccone G, Palacios T, Neumaier D, Seabaugh A, Banerjee S K and Colombo L 2014 *Nat. Nanotechnol.* **9** 768–79
- [29] Ataei S S, Varsano D, Molinari E and Rontani M 2021 *Proc. Natl Acad. Sci. USA* **118** e2010110118
- [30] Keldysh L 1979 *Sov. Phys - JETP* **29** 658
- [31] Ataei S S and Sadeghi A 2021 *Phys. Rev. B* **104** 155301
- [32] Murakami Y, Golež D, Kaneko T, Koga A, Millis A J and Werner P 2020 *Phys. Rev. B* **101** 195118
- [33] Golež D, Sun Z, Murakami Y, Georges A and Millis A J 2020 *Phys. Rev. Lett.* **125** 257601
- [34] Tanabe T, Kaneko T and Ohta Y 2021 *Phys. Rev. B* **104** 245103
- [35] Kaneko T, Sun Z, Murakami Y, Golež D and Millis A J 2021 *Phys. Rev. Lett.* **127** 127402
- [36] Sun Z and Millis A J 2021 *Phys. Rev. Lett.* **126** 027601
- [37] Crépeel V and Fu L 2021 arXiv:2103.12060